2016 IEEE/RSJ International Conference on Intelligent Robots and Systems (IROS)
Daejeon Convention Center
October 9-14, 2016, Daejeon, Korea

Adaptive 3D Pose Computation of Suturing Needle Using Constraints From Static Monocular Image Feedback

Fangxun Zhong, David Navarro-Alarcon, Zerui Wang, Yun-hui Liu, Tianxue Zhang, Hiu Man Yip and Hesheng Wang

***Abstract*— In this paper, we address the problem of the image-based 3D pose computation of a semi-circle suturing needle using monocular image feedback for laparoscopy. We propose a constrained two-degree-of-freedom (2-DOF) geometry-based modelling method to parametrise the needle's 6-DOF pose, including depth information. The modelling solely relies on the simultaneous observation of the needle's apparent tip and junction. No external markers are needed for extra constraints. An adaptive controller combining gradient descent and vector-flow method is introduced to iteratively guide the needle's initial guessing pose to its real pose by minimizing image-based position errors. Experiments have been conducted using both numerical simulations and simulated laparoscopic scenarios to evaluate the performance of the algorithm.**

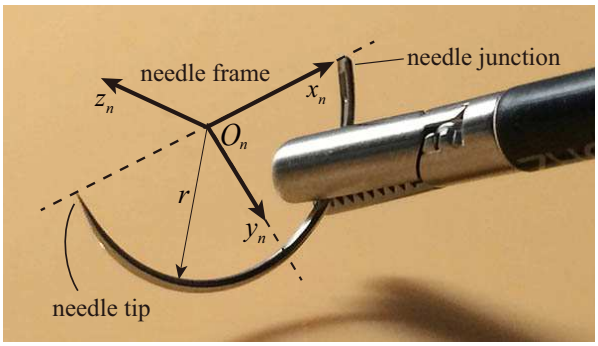

Fig. 1: Assignment of the needle frame $\mathcal{F}_n$ fixed on the needle.

I. INTRODUCTION

Minimally invasive surgery (MIS) has nowadays been widely preferred by patients due to its reduction of the incision size and postoperative recovery time. In laparoscopy, for example, small incision holes are made on the patient's body for the insertion of surgical instruments into the torso. The surgeon then has to rely on the image view from a laparoscope. Because of the compact operating space, dexterous procedures like suturing are among some of the difficult tasks during MIS [1]. The accuracy of handling the suturing needle is critically affected by the apparent pose observed from laparoscope's image feedback. Meanwhile, as robot-assisted surgery reaches increasing popularity, visual aids for needle pose recovery are significant for robotic assistances like needle trajectory planning [2], needle-tissue interaction [3] and automated suturing [4]. In this paper, we aim to develop an algorithm to adaptively compute the 3D pose of the suturing needle using a single frame of image feedback from a monocular laparoscope.

Generally, using a 3D laparoscope enables explicit computation method in stereo vision to determine a feature point's 3D position [5]. However, those algorithms fail to be implemented on a conventional monocular laparoscope, which remains the most commonly used type of camera as source of image feedback for MIS. The major issue of 3D pose computation using monocular camera is the loss of depth information especially for point-based pose modelling. The degenerated 2D information cannot provide enough constraints to determine positions in 3D space unless extra conditions are introduced.

There are related works that address the pose recovery issue of a suturing needle for MIS. For example, Nageotte et al. introduces a pose determination method in [6] by adding auxiliary pose knowledge of the needle holder, i.e. a surgical forceps with cylindrical structure. Both works in [6] and [7] suggest needle be painted (e.g. in green) and use the needle's 2D contour as direct pose feedback. To avoid modifying the natural property of the needle, Wengert et al. [8] propose a simple homography-based pose computation method by regarding the gripping point of the surgical forceps on the needle as a virtual marker. Furthermore, Chang [9] implements Artificial Neural Network for needle recognition from stereo images. A RANSAC-based circle fitting algorithm is then implemented to determine the centre of the circle containing the suturing needle.

To contribute to such pose computation problem with minimal modification of surgical tools, in this paper, we introduce a new 3D pose computation method to determine pose of a semi-circle suturing needle. Unlike other approaches that require modified features, our modelling only requires simultaneous observation of the needle tip and junction point (since the surgeon usually handles the needle by gripping its body during suturing). We then propose a geometry-based pose modelling to constrain the possible 3D pose of the needle, including depth information, with only two newly-defined rotational DOFs. To compute the exact pose, an adaptive algorithm integrating gradient descent and vector-flow analysis is presented to iteratively drive

FZ, DNA, ZW, YL, TZ and H.M.Y are with the Department of Mechanical and Automation Engg., The Chinese University of Hong Kong, HKSAR, China. HW is with the Department of Automation, Shanghai Jiao Tong University, China. Corresponding author's e-mail: fxzhong@mae.cuhk.edu.hk.

This work is supported in part by the HK RGC under grants 415011 and CUHK6/CRF/13G, by the HK ITF under grants ITS/112/15FP and ITT/012/15GP, by the VC's Discretionary Fund through CURI grant 4930763 and 4930725, and by the CUHK SHIAE under grant 8115053.

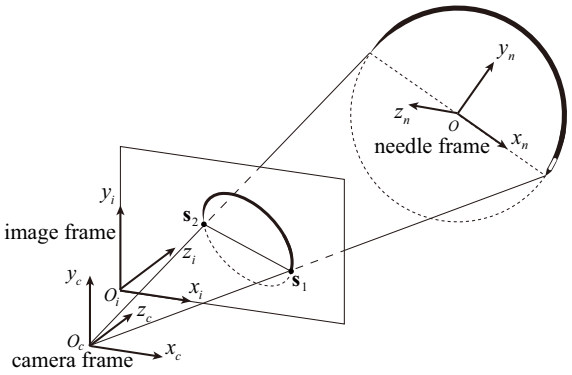

Fig. 2: Notations of camera frame $\mathcal{F}_c$, image frame $\mathcal{F}_i$ and needle frame $\mathcal{F}_n$.

the guessing pose of the virtual needle to its real pose. The controller's feedback can simply be the centroid of the recovered apparent curve of the needle's body. Experiments based on simulation of laparoscopic scenarios are presented for performance evaluation.

The structure of this paper is organised as follows: Section II introduces the basic modelling of both the camera and needle; Section III presents the modelling and exact pose computation of the needle using the constrained 2DOF parametrising model; Section IV presents the control algorithm to compute the genuine pose of the needle; in Section V experiment results are reported; conclusions are drawn in Section VI.

II. MODELLING

A. Perspective Projection of Camera

Consider a monocular camera that observes a world feature point described by $\mathbf{p}_i \in \mathbb{R}^3$ with respect to the camera frame denoted by $\mathcal{F}_c$, whose origin coincides with the optic centre. Then it is well-known that the point's perspective projection in camera frame can be computed as follows:

$$\begin{bmatrix}\mathbf{s}_i \\ 1\end{bmatrix} = \frac{1}{z_i}\mathbf{C}\mathbf{p}_i \tag{1}$$

where $\mathbf{s}_i \in \mathbb{R}^2$ is the projected 2D point on the image plane; the scalar z_i denotes the depth of the point (the distance along z-axis of the camera frame); the calibration matrix $\mathbf{C} \in \mathbb{R}^{3\times3}$ contains the intrinsic parameters of the laparoscopic camera. In this paper, we assume the matrix $\mathbf{C}$ is calibrated without lens distortions.

B. Needle Geometry

Consider a semi-circle suturing needle (or 1/2 circle needle) used in laparoscopy, we call the circle that contains the curve of the needle arc as the "needle circle". Then the centre of this circle locates exactly at the midpoint of the connected segment between needle's tip and junction point. Here we assign a new 3D coordinate frame $\mathcal{F}_n$ fixed on the needle, namely the needle frame, whose origin coincides with the centre of the needle circle and its x-axis pointing to the junction (see Fig. 1 for complete assignment). Thus, there exists a transformation between frame $\mathcal{F}_n$ and frame $\mathcal{F}_c$ which can be described as follows:

$$\begin{bmatrix}\mathbf{p}_i \\ 1\end{bmatrix} = {}^c\mathbf{T}_n \begin{bmatrix}{}^n\mathbf{p}_i \\ 1\end{bmatrix} \tag{2}$$

where ${}^n\mathbf{p}_i$ denotes the coordinate of a camera-visible point in 3D space relative to frame $\mathcal{F}_n$; the homogeneous transformation matrix ${}^c\mathbf{T}_n \in \mathbb{R}^{4\times4}$ contains the complete pose information of the needle with respect to camera. In our model, we assume that both the tip and junction (two endpoints) of the suturing needle can be observed by the camera to provide point-based constraints for pose computation. The size of the circle, i.e. the radius *r* of the needle circle, is exactly known.

Note, importantly, that the perspective projection of a circle in 3D space is a perfect ellipse on the image plane [10]. Hence, the projection of the semi-circle needle on a 2D plane is a partial ellipse curve. Note also that a surgical gripper is used to handle the needle, thus the needle is only partially visible.

Problem statement. Given the intrinsic parameters by a calibrated matrix $\mathbf{C}$ and the radius *r* of the needle circle, develop an algorithm to compute the needle's 3D pose, i.e. the transformation matrix ${}^c\mathbf{T}_n$ from a single frame of image captured by a monocular laparoscopic camera.

III. POSE PARAMETRISATION

A. A Constrained 2-DOF Pose Modelling

In this subsection, we propose a 2-DOF modelling method to represent the rotation and orientation of the suturing needle using image-based constraints. Denote the projected points of the needle's tip and junction on the image plane by $\mathbf{s}_i \in \mathbb{R}^2$ (for i = 1, 2). With the knowledge of matrix $\mathbf{C}$, one can compute the vector representing the 2D feature point in 3D camera frame using, described by $\mathbf{c}_i$ (for i = 1, 2), as follows:

$$\mathbf{c}_i = f\mathbf{C}^{-1}\begin{bmatrix}\mathbf{s}_i^T & 1\end{bmatrix}^T \tag{3}$$

where $\mathbf{c}_i \in \mathbb{R}^3$, f is the known focal length. The feedback of $\mathbf{s}_1$ and $\mathbf{s}_2$ from the captured image suggests that the real 3D positions of the needle junction and tip lie on the two rays spanned from the camera origin through $\mathbf{c}_1$ and $\mathbf{c}_2$, represented by l_1 and l_2, respectively. If the estimated positions of the needle junction and tip are denoted by p_1 and p_2, then their 3D coordinates with respect to frame $\mathcal{F}_c$ can be described by vector $\mathbf{m}_1$ and $\mathbf{m}_2$, and can be computed as follows:

$$\mathbf{m}_i = \lambda_i \frac{\mathbf{c}_i}{\|\mathbf{c}_i\|} \tag{4}$$

where λ_i (i = 1, 2) is a scalar parametrising the vector $\mathbf{m}_i$. To map q_1 to λ_i, we compute the angle of vector $\mathbf{h} = \overrightarrow{p_1p_2}$ relative to $\mathbf{m}_1$ using both dot and cross product computation:

$$\cos q_1 = \frac{\mathbf{m}_1 \cdot \mathbf{h}}{\|\mathbf{m}_1\|\|\mathbf{h}\|}, \quad \sin q_1 = \frac{\|\mathbf{m}_1 \times \mathbf{h}\|}{\|\mathbf{m}_1\|\|\mathbf{h}\|\|\mathbf{n}\|} \tag{5}$$

where q_1 is the angle, $\mathbf{n}$ is the unit vector perpendicular to $\mathbf{m}_1$ and $\mathbf{h}$. Note that the vector $\mathbf{h}$ actually contains the partial

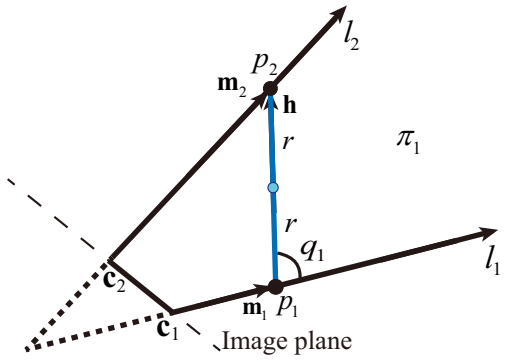

Fig. 3: The orthogonal view of the sliding plane.

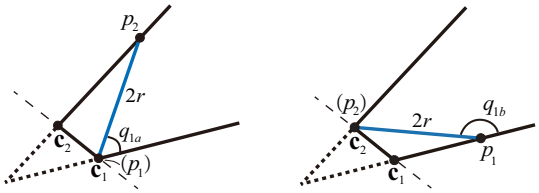

(a) q_1 at minimum (q_{1a}). (b) q_1 at maximum (q_{1b}).

Fig. 4: Two extreme poses of q_1 on the sliding plane (green point for junction and red point for tip).

pose of the needle circle, and always belongs to the plane π_1 formed by l_1 and l_2, since $\mathbf{m}_1$ and $\mathbf{m}_2$ slide along l_1 and l_2 respectively regardless of their real positions. Thus, we call π_1 as a 'sliding plane' (shown in Fig. 3). Furthermore, (5) with (4) could be written into linear form in terms of λ_i:

$$\begin{bmatrix}\cos q_1\\ \sin q_1\end{bmatrix} = \mathbf{H}\begin{bmatrix}\lambda_1\\ \lambda_2\end{bmatrix} \tag{6}$$

where $\mathbf{H} \in \mathbb{R}^{2\times 2}$ is a constant matrix and equals to:

$$\mathbf{H} = \begin{bmatrix}\frac{-\mathbf{c}_1\cdot\mathbf{c}_1}{2r\|\mathbf{c}_1\|^2} & \frac{\mathbf{c}_1\cdot\mathbf{c}_2}{2r\|\mathbf{c}_1\|\|\mathbf{c}_2\|}\\ 0 & \frac{\mathbf{c}_1\times\mathbf{c}_2}{2r\|\mathbf{c}_1\|\|\mathbf{c}_2\|}\end{bmatrix} \tag{7}$$

Remark 1. The computation in (5) assumes that $\sin q_1$ should be positive, which is always satisfied since the needle's position never enters the back of imaging sensor. Thus, there exists a solvable range $q_1 \in (q_{1a}, q_{1b})$ which is a proper subset of $q_1 \in (0, \pi)$ that guarantees the positiveness of q_1. Fig. 4 illustrated the two particular poses of the needle when q_1 reach the limits due to above concerns.

Proposition 1. The matrix $\mathbf{H}$ has a rank of 2 as long as $\mathbf{s}_1$ and $\mathbf{s}_2$ (i.e. $\mathbf{c}_1$ and $\mathbf{c}_2$ in $\mathcal{F}_c$) doesn't coincide with each other.

Proof: By calculating the determinant, we obtain the following:

$$|\,\mathbf{H}\,| = -\frac{\lambda_2(\mathbf{c}_1\cdot\mathbf{c}_1)(\mathbf{c}_1\times\mathbf{c}_2)}{4r^2\|\mathbf{c}_1\|^3\|\mathbf{c}_2\|} \tag{8}$$

which is a non-zero value subject to $\mathbf{c}_1 \times \mathbf{c}_2 \neq \mathbf{0}$. The fact that $\lambda_1, \lambda_2 \neq 0$ guarantees (6) have realistic solutions.

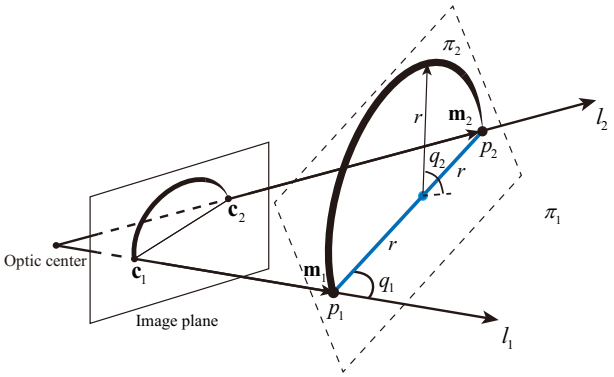

Fig. 5: The complete 2-DOF pose parametrisation of the needle.

Now, since the origin of the needle frame always locates on the midpoint of the line segment $\overline{p_1p_2}$, the position of the needle frame can be described as follows:

$${}^c\mathbf{t}_n = \frac{1}{2}(\mathbf{m}_1 + \mathbf{m}_2) = \mathbf{L}\begin{bmatrix}\lambda_1\\ \lambda_2\end{bmatrix} \tag{9}$$

where ${}^c\mathbf{t}_n \in \mathbb{R}^3$ depicts the position of frame $\mathcal{F}_n$ relative to frame $\mathcal{F}_c$; the matrix $\mathbf{L} \in \mathbb{R}^{3\times 2}$ contains information of $\mathbf{c}_1$ and $\mathbf{c}_2$ and transforms λ_i to ${}^c\mathbf{t}_n$. By substituting (9) into (6), we have

$${}^c\mathbf{t}_n = \mathbf{L}\mathbf{H}^{-1}\begin{bmatrix}\cos q_1\\ \sin q_1\end{bmatrix} \tag{10}$$

The result in (10) indicates a single mapping from q_1 to ${}^c\mathbf{t}_n$. This states an important point that, the 3D position of the needle frame $\mathcal{F}_n$ with respect to the camera can be uniquely determined by a single scalar q_1. It generates constraints along the rotational DOFs of frame $\mathcal{F}_n$ as well. Here we introduce q_1 as a new independent rotational DOF to parametrise the pose of the needle from image constraints.

To complete the pose description, we first randomly select a scalar $\theta_r \in \mathbb{R}^3$ subject to $\theta_r \in (0, \pi)$, then an arbitrary point located on the circle can be determined, with its coordinate ${}^n\mathbf{p}_r$ relative to frame $\mathcal{F}_n$ described as follows:

$${}^n\mathbf{p}_r = \begin{bmatrix}r\cos\theta_r & r\sin\theta_r & 0\end{bmatrix}^T \tag{11}$$

Let us denote the plane containing the needle circle by π_2, the unit normal vector of plane π_2 can be obtained as follows:

$$\mathbf{n}_n = \frac{\mathbf{h}\times{}^n\mathbf{p}_r}{\|\mathbf{h}\times{}^n\mathbf{p}_r\|} \tag{12}$$

where $\mathbf{n}_n$ is the computed unit normal vector. Now we compute the dihedral angle q_2 between the plane π_1 and plane π_2 as follows:

$$\cos q_2 = \frac{\mathbf{n}\cdot\mathbf{n}_n}{\|\mathbf{n}\|\|\mathbf{n}_n\|} \tag{13}$$

Here we regard q_2 as the second independent DOF representing the pose of the needle. The vector $\mathbf{n}$ is the unit vector perpendicular to the plane π_2 obtained from (5). Fig. 5 shows the conceptual description of the pose representation.

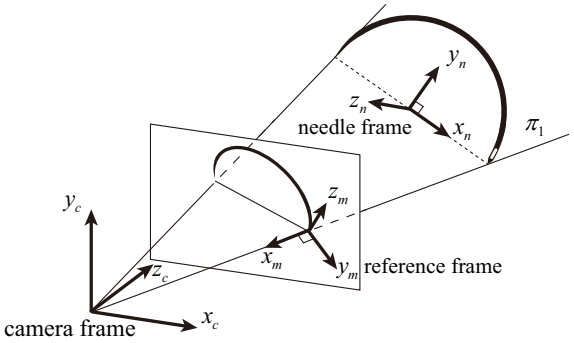

Fig. 6: The illustrated reference frame $\mathcal{F}_m$ in 3D space.

B. Total Pose Parametrisation

Now we derive the pose of the needle relative to the camera under new parametrisation model. First we introduce a reference frame denoted by $\mathcal{F}_m$, whose origin coincides with point $\mathbf{c}_1$ and the x-axis points along the negative direction of vector $\mathbf{c}_1$. The y-axis lies in plane π_1, leaving z-axis the unit normal vector of π_1 (Fig. 6). Then, we transform from frame $\mathcal{F}_m$ to $\mathcal{F}_c$ using the following homogeneous transformation:

$$ {}^c\mathbf{T}_m = \begin{bmatrix} {}^c\mathbf{R}_m & \mathbf{c}_1 \\ \mathbf{0}_{1\times 3} & 1 \end{bmatrix}_{4\times 4} \tag{14} $$

where ${}^c\mathbf{R}_m \in \mathbb{R}^{3\times 3}$ is a rotation matrix and can be further computed as follows:

$$ {}^c\mathbf{R}_m = \begin{bmatrix} \mathbf{x}_m & \frac{\mathbf{n}\times\mathbf{x}_m}{\|\mathbf{n}\times\mathbf{x}_m\|} & \mathbf{n} \end{bmatrix} \tag{15} $$

where $\mathbf{x}_m$ is a unit vector equals to $-\frac{\mathbf{c}_1}{\|\mathbf{c}_1\|}$.

Finally, by denoting the following vector $\mathbf{q} \in \mathbb{R}^2$:

$$ \mathbf{q} = \begin{bmatrix} q_1 & q_2 \end{bmatrix}^T \tag{16} $$

we complete the pose parametrisation by computing the pose transformation matrix from frame $\mathcal{F}_n$ to $\mathcal{F}_c$:

$$ {}^c\mathbf{T}_n = \begin{bmatrix} {}^c\mathbf{R}_m\, {}^m\mathbf{R}_n(\mathbf{q}) & {}^c\mathbf{t}_n \\ \mathbf{0}_{1\times 3} & 1 \end{bmatrix} \tag{17} $$

where ${}^m\mathbf{R}_n \in \mathbb{R}^{3\times 3}$ is a rotation matrix containing variables of q_1 and q_2 only, i.e.

$$ {}^m\mathbf{R}_n(\mathbf{q}) = \begin{bmatrix} \cos q_1 & -\sin q_1 \cos q_2 & \sin q_1 \sin q_2 \\ \sin q_1 & \cos q_1 \cos q_2 & -\cos q_1 \sin q_2 \\ 0 & \sin q_2 & \cos q_2 \end{bmatrix} \tag{18} $$

Note that the position vector ${}^c\mathbf{t}_n$ can be determined from (10). Hence, by using constraints derived from the image feedback, the 3D pose of the suturing needle with respect to camera frame $\mathcal{F}_c$ has now been fully transformed into a 2-DOF pose parametrisation using only q_1 and q_2. Once the exact values of q_1 and q_2 are solved, the matrix ${}^c\mathbf{T}_n$ can be uniquely determined from (10) and (17).

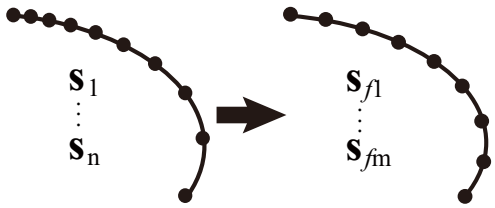

Fig. 7: The position homogenisation of the projected points from $\mathbf{s}$ to $\mathbf{s}_f$.

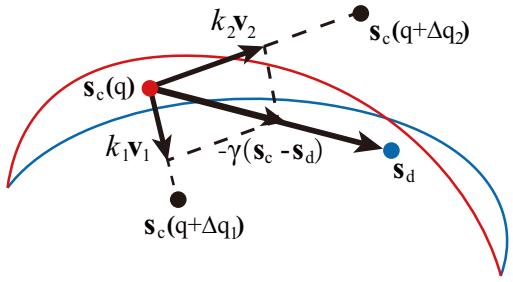

Fig. 8: The illustrated error input for the controller design (red for current pose and blue for desired pose).

IV. Adaptive Pose Computation

In this sub-section, we propose an iterative algorithm to compute the genuine pose of the needle from the camera inspired from [11]. Based on new parametrisation, a possible range of the needle's pose has been discussed previously in Fig. 4. Let us assign an initial guessing pose of the virtual adaptive needle at first. Extra constraints are then needed to adjust q_1 and q_2 so that the needle will move to its real pose.

Here, we simply calculate the centroid of the needle's fitted apparent curve on the image plane as a 2D constraint to regulate the 2-DOF pose variables. Depict the needle's instant pose by q_1 and q_2, then an arbitrary sampling point on the needle is described as follows:

$$ {}^n\mathbf{f}_i = \begin{bmatrix} rcos(\theta) & rsin(\theta) & 0 & 1 \end{bmatrix}^T \tag{19} $$

where θ is the parametric variable. If n points are sampled from the needle, the ith point has its projection calculated from (1):

$$ \mathbf{s}_{fi} = \frac{1}{z_i} \begin{bmatrix} \mathbf{C} \mid \mathbf{0}_{3\times 1} \end{bmatrix} {}^c\mathbf{T}_n\, {}^n\mathbf{f}_i \tag{20} $$

where the depth information z_i can be directly computed using the instant pose of the adaptive needle. Then the centroid of the adaptive needle can be simply computed:

$$ \mathbf{s}_c(q_1, q_2) = \frac{1}{m} \sum_{j=1}^{m} \mathbf{s}_{fj} \tag{21} $$

where $\mathbf{s}_c \in \mathbb{R}^2$. Note that since the uniformly-distributed sampling points on the circle will generate non-uniform projected points on the image, thus m is the number of points actually used instead of n. Either eliminations or interpolations are applied to homogenise the positions of the projected points (see representation in Fig. 7).

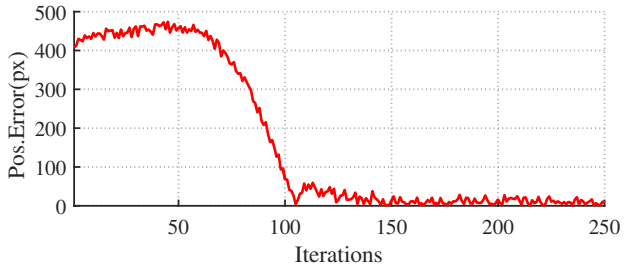

Fig. 9: The magnitude of position error ${}^{c}t_n$ in pixels from numerical simulation (with noise).

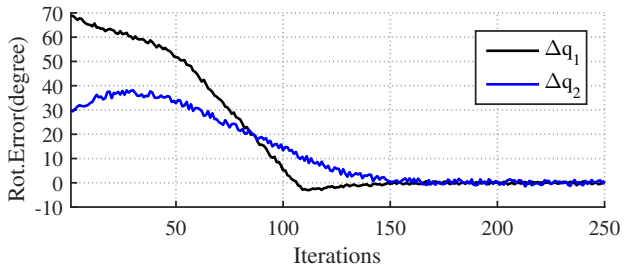

Fig. 10: The magnitude of rotation errors q_1 and q_2 in degrees from numerical simulation (with noise).

To achieve the pose correction of our algorithm, we define the following cost function:

$$J(\mathbf{q}) = \frac{1}{2}\|\mathbf{s}_c(\mathbf{q}) - \mathbf{s}_d\|^2 \tag{22}$$

where $\mathbf{s}_c(\mathbf{q})$ is the centroid of the recovered needle curve observed from camera. Then we propose an updating rule as follows:

$$\frac{dq_i}{dt} = -\mathbf{\Gamma}\{\frac{\partial J}{\partial q_i} + \frac{1}{k_i}(\frac{\partial \mathbf{s}_c}{\partial q_i})^T\mathbf{v}_i\} \tag{23}$$

where $\mathbf{\Gamma} \in \mathbb{R}^{2\times 2}$ is a positive-definite gain matrix. The first term $\frac{\partial J}{\partial \mathbf{q}}$ in (23) comes from gradient descent method. The second term yields a vector-flow based updating rule. Discretely, a differential motion Δq_i (i=1, 2) in a single time step generates an instant motion vector $\mathbf{v}_i \in \mathbb{R}^2$ with following form:

$$\mathbf{v}_i = \mathbf{s}_c(\Delta q_i) - \mathbf{s}_d = \frac{\partial \mathbf{s}_c}{\partial q_i}\Delta q_i \tag{24}$$

where $\frac{\partial \mathbf{s}_c}{\partial q_i} \in \mathbb{R}^2$ can be numerically computed in the experiment. To guide the point $\mathbf{s}_c$ to the desired position $\mathbf{s}_d$, we compute the vector additionally using the parallelogram law (Fig. 8):

$$k_1\mathbf{v}_1 + k_2\mathbf{v}_2 = -\gamma(\mathbf{s}_c(\mathbf{q}) - \mathbf{s}_d) \tag{25}$$

where γ is the updating gain for vector-flow adjustment. The scalar k_i can be computed from (25). Note that the range constraints of q_1 reduce its possibility to reach local minima.

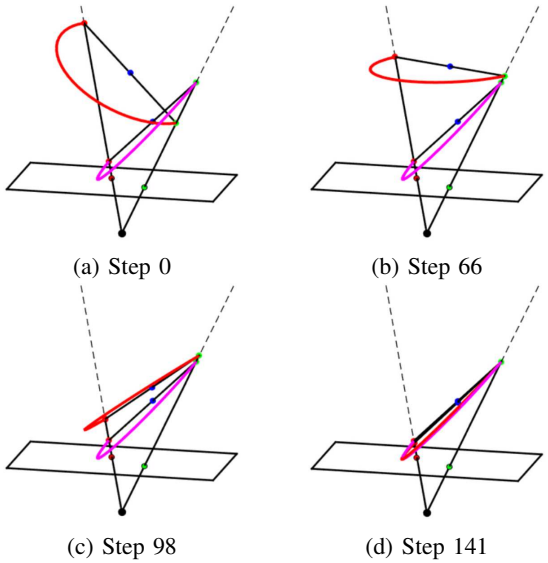

(a) Step 0 (b) Step 66

(c) Step 98 (d) Step 141

Fig. 11: The result of the pose computation after iterations.

V. EXPERIMENTS

A. Numerical Simulations

We first conduct numerical simulations in MATLAB R2015b to evaluate the performance of our algorithm. We assume a virtual imaging sensor with the size of 1600×800 pixels (px) and has a focal length of 400px. The size of the semi-circle suturing needle to be observed has a radius of 600px. The initial position is set to $[q_1 \;\; q_2]^T = [90 \;\; 90]^T$ in degrees. The gain elements in $\mathbf{\Gamma}$ are set to (0.012 , 0.01) to ($\frac{dq_1}{dt}$, $\frac{dq_2}{dt}$) respectively. Each iteration step is set to 0.01s. In addition, we add uniform random noise to the desired pose of the needle to simulate more realistic scenarios like rough image processing results ($\pm 1^\circ$ for q_1 and $\pm 1.5^\circ$ for q_2).

Fig. 11 shows the result of iterative pose computation using the above configurations. The adaptive needle with an initial guessing pose converges to its real pose after limited times of iteration (adjustable by gain values) using the proposed updating rule. The observed needle junction and tip determine the sliding plane in 3D space, on which the origin of the needle frame is located. The centroids provide image-based error input for the pose correction process. The noise added on the real pose doesn't affect its convergent performance. The error trajectories of the pose computation are shown in Fig. 9 and Fig. 10.

B. Pose Computation Using Image Feedback

We use the monocular mode of the Karl Storz® 3D laparoscope as image source. The intrinsic parameters are calibrated using method in [12]. We use a semi-circle suturing needle with the size of 7mm in radius for laparoscopy, which is gripped by a surgical forceps during experiments. Both the laparoscope and the surgical instrument are handled by hands. The algorithm assumes the centroid of the needle's apparent curve can be calculated using recovered curve, which allows partial occlusion of the needle by the forceps. Furthermore, we keep the gains for updating $\mathbf{q}$ as adopted

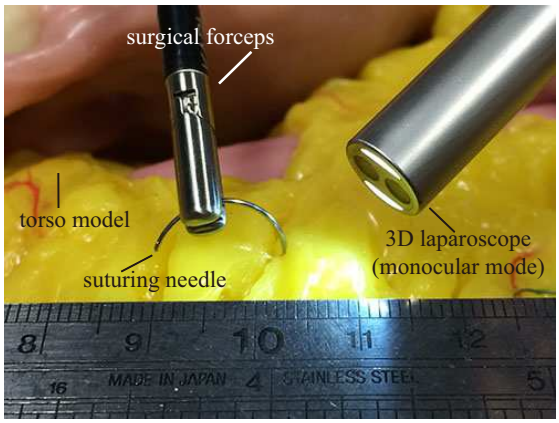

Fig. 12: The experimental set-up.

in numerical simulations, and the needle's initial pose is set to $[q_1 \quad q_2]^T = [60 \quad 90]^T$. The set-up of the experiments is shown in Fig. (12).

We demonstrate in this paper two cases of the needle's pose computation results from our experiments, namely Case 1 and Case 2. The computed 6-DOF poses of the needle with respect to the camera are shown in Table. I. Fig. 13(a) and (b) illustrate the pose recovery results using real captured images. The projection of the adaptive needle overlaps the captured one in the real image.

TABLE I: TWO DEMONSTRATED POSE COMPUTATION RESULTS

	${}^c\mathbf{R}_n$			${}^c\mathbf{t}_n$ (mm)
$Case\ 1$	0.533	0.831	−0.159	4.589
	0.566	−0.490	−0.664	−10.200
	−0.629	0.264	−0.731	20.450
$Case\ 2$	0.211	−0.960	0.187	−4.827
	0.940	0.147	−0.310	1.774
	0.267	0.241	0.933	14.678

VI. CONCLUSIONS

In this paper, we introduced a new pose modelling method to compute the pose of a semi-circle suturing needle using a monocular laparoscope. The modelling parametrises the 6-DOF pose of the needle by only two variables. We proposed a gradient descent method with vector-flow computation to iteratively guide the pose of the needle using image-based errors from a single image frame. We finally evaluated the method using experiments from both numerical simulations and image-based pose computation.

The core idea in this approach is to use image feedback to generate pose correction motion with the proposed control law. Our experiments show that it can work with small perturbations. We suggest the method to be used with image processing algorithms to obtain effective image features.

In our future work, we will further evaluate this approach combined with image processing to obtain fitted curves from the laparoscopic image. Meanwhile, we will study the automatic 3D positioning problem of the needle using medical robots for robot-assisted suturing.

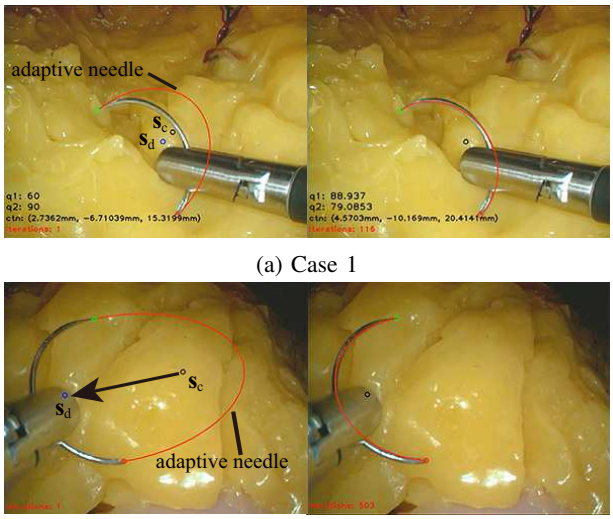

(a) Case 1

(b) Case 2

Fig. 13: The pose computation using real images.

REFERENCES

[1] M. C. Çavuşoğlu, F. Tendick, M. Cohn, and S. S. Sastry, "A laparoscopic telesurgical workstation," *IEEE Trans. Robotics and Automation*, vol. 15, no. 4, pp. 728–739, 1999.

[2] F. Nageotte, P. Zanne, M. De Mathelin, and C. Doignon, "A circular needle path planning method for suturing in laparoscopic surgery," in *Proc. IEEE Int. Conf. Robotics and Automation*. IEEE, 2005, pp. 514–519.

[3] Y. Tian, Y. Yang, X. Guo, and B. Prabhakaran, "Haptic simulation of needle-tissue interaction based on shape matching," in *IEEE Int. Symp. Haptic, Audio and Visual Environments and Games (HAVE)*. IEEE, 2014, pp. 7–12.

[4] S. Leonard, K. L. Wu, Y. Kim, A. Krieger, and P. C. Kim, "Smart tissue anastomosis robot (star): a vision-guided robotics system for laparoscopic suturing," *IEEE Trans. Biomedical Engineering*, vol. 61, no. 4, pp. 1305–1317, 2014.

[5] R. Hartley and A. Zisserman, *Multiple view geometry in computer vision*. Cambridge university press, 2003.

[6] F. Nageotte, C. Doignon, M. de Mathelin, P. Zanne, and L. Soler, "Circular needle and needle-holder localization for computer-aided suturing in laparoscopic surgery," in *Medical Imaging*. International Society for Optics and Photonics, 2005, pp. 87–98.

[7] Y. Kurose, Y. M. Baek, Y. Kamei, S. Tanaka, K. Harada, S. Sora, A. Morita, N. Sugita, and M. Mitsuishi, "Preliminary study of needle tracking in a microsurgical robotic system for automated operations," in *Proc. IEEE Int. Conf. Control, Automation and Systems (ICCAS)*. IEEE, 2013, pp. 627–630.

[8] C. Wengert, L. Bossard, C. Baur, G. Székely, and P. C. Cattin, "Endoscopic navigation for minimally invasive suturing," *Computer Aided Surgery*, vol. 13, no. 5, pp. 299–310, 2008.

[9] J. Chang, "Robust needle recognition using artificial neural network (ann) and random sample consensus (ransac)," in *Applied Imagery Pattern Recognition Workshop (AIPR)*. IEEE, 2012, pp. 1–3.

[10] R. Safaee-Rad, I. Tchoukanov, K. C. Smith, and B. Benhabib, "Three-dimensional location estimation of circular features for machine vision," *IEEE Trans. Robotics and Automation*, vol. 8, no. 5, pp. 624–640, 1992.

[11] D. Navarro-Alarcon, Z. Wang, H. M. Yip, Y.-h. Liu, F. Zhong, T. Zhang, J. Shi, and H. Wang, "Robust image-based computation of the 3d position of rcm instruments and its application to image-guided manipulation," in *Proc. IEEE Int. Conf. Robotics and Automation*. IEEE, 2016, pp. 4115–4121.

[12] Z. Zhang, "A flexible new technique for camera calibration," *IEEE Trans. Pattern Analysis and Machine Intelligence*, vol. 22, no. 11, pp. 1330–1334, 2000.